ELSEVIER

International Journal of Adhesion & Adhesives 21 (2001) 445–453

International Journal of Adhesion & Adhesives

www.elsevier.com/locate/ijadhadh

Understanding and control of adhesive crack propagation in bonded joints between carbon fibre composite adherends II. Finite element analysis

F.J. Guild, K.D. Potter*, J. Heinrich, R.D. Adams, M.R. Wisnom

Faculty of Engineering, University of Bristol, Queen's Building, University Walk, Bristol BS8 1TR, UK

Accepted 29 March 2001

Abstract

Carbon fibre composites are being widely considered for many classes of heavily loaded components. A common feature of such components is the need to introduce local or global loads into the composite structure. The use of adhesive bonding rather than mechanical fasteners offers the potential for reduced weight and cost. However, such bonded joints must be shown to behave in a predictable and reliable way. A major aspect of this is to demonstrate that the progress of cracks through the bonds is well understood. The simulation work presented here complements the experimental work presented in Part I. The observed failure processes and their sequence are successfully described and modelled. © 2001 Elsevier Science Ltd. All rights reserved.

Keywords: B. Composites; C. Finite element stress analysis; D. Fracture

1. Introduction

Finite element modelling can be a useful tool in the understanding of the behaviour of adhesive joints, especially when it is combined with an extensive experimental programme. The experimental programme carried out in this programme is described in Part I of this paper [1]. It has been shown to be possible to modify adhesively bonded joints between composite adherends such that failure is contained within the bond line and does not propagate into the composite laminate. This was achieved by modification of the bond line using additional material, either continuous film or woven cloth placed along the centre of the bondline, or discontinuous particulate material introduced along the interface below which delamination is expected to occur. The successful modification of joints such that failure occurs via this mechanism, allowing the crack growth to be far more readily monitored, is a crucial step to allowing more widespread use of adhesively bonded composite structures.

Finite element simulations of the joints have been carried out. The results of these simulations have been used to describe and confirm the experimental observations. Experimental observations, particularly the observed direction of crack propagation, have been incorporated into the models. This paper presents the finite element results and comparisons with the experimental results reported in Part I [1].

2. Joint preparation

The adherends consisted of unidirectional carbon fibre laminate, with the fibre axis parallel to the axial direction of the joint. The carbon fibre laminate was manufactured from Hexcel 914C-TS prepreg using an autoclave. The adhesive used was a single-part hot-cured modified epoxy paste, EC3448, from 3M; this adhesive has been used in previous work, e.g. [2].

The overall geometry of the joint is shown in Fig. 1; the section is shown in the through-thickness direction; the joint width was 20 mm. The inner adherends were 8 mm thick and the outer adherends were 4 mm thick. The overlap length was 30 mm (excluding fillets). Reverse chamfers and adhesive fillets were used at the

*Corresponding author. Tel.: +44-0117-928-9155; fax: +44-0117-927-2771.

E-mail addresses: k.potter@bris.ac.uk (K.D. Potter).

PII: S0143-7496(01)00021-5

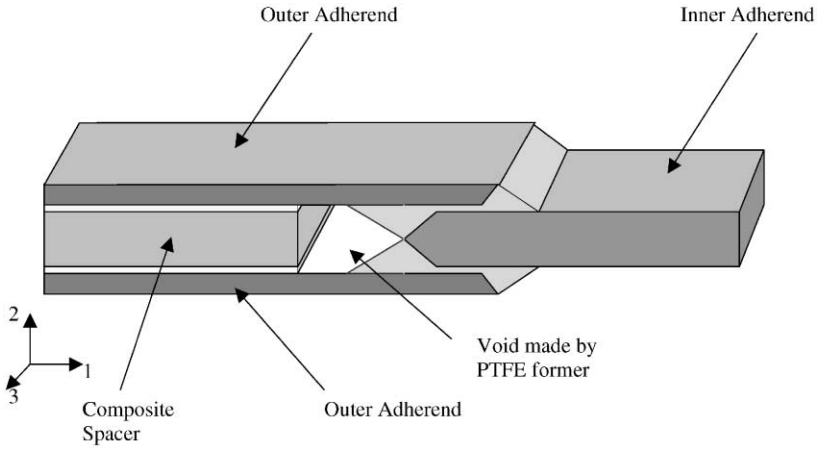

Fig. 1. Schematic of double-lap joint.

ends of the bondline; these geometric features reduce the through-thickness stress and reduce the occurrence of premature failure of the joint via transverse failure of the composite laminate [3]. The external fillet angle was 20° and the angle of the reverse chamfer was 30° (angles with respect of the horizontal, axial, direction). The adhesive thickness was 0.7 mm. The joints were carefully prepared using a jig to ensure good alignment and accurate bondlines.

The adhesive joints were modified by the addition of nylon cloth or Kapton™ film, which was placed along the centre of the bondline. As described in Part I [1] modifications using powders were also tested in the experimental programme but these joints were not included in the fatigue testing programme and have not been analysed here.

3. Experimental programme

The experimental programme was centred on fatigue testing of balanced, double-lap shear joints. In addition to the fatigue tests, some quasi-static tests were carried out. The same modes of failure for the different joints were found for both types of testing.

For unmodified joints, failure was observed to initiate in the adhesive layer at the corner of the fillet. The crack grew towards the opposite adherend, final failure occurred via delamination of the adherend. Introduction of the cloth or film along the centre of the bondline lead to crack deflection; delamination of the adherend was prevented. For joints modified using the lighter weight nylon cloth, failure loads were reduced by approximately 20% compared with the unmodified joints. For joints modified using the Kapton™ layer, no reduction in failure load was measured. Fatigue testing of these joints indicated that a stable region of crack growth within the adhesive layer occurred for the modified joints, in contrast to the catastrophic sudden failure via adherend delamination found for the unmodified joints.

4. Finite element analysis

The finite element analysis was carried out using ABAQUS version 5.7 running on a SGI O2 workstation. The meshes were drawn using PATRAN version 7.5, with some manual editing of the data files. Post processing was carried out using ABAQUS POST.

4.1. Mesh

Examination of the experimental results [1] showed that the failure processes appear to initiate along the centre-line of the joint, so the mesh was drawn in 2-dimensions in the axial-thickness plane (1–2 plane shown in Fig. 1) using plane strain elements, modelling an inner slice of the joint. These elements impose zero strain but allow finite stress in the out-of-plane (through-width) direction (3-direction shown in Fig. 1).

The overall geometry of the finite element models is shown in Fig. 2. The double-lap joint is symmetric so only half the joint is modelled. The boundary conditions at the ends represent built-in conditions; constraint in the 2-direction (through-thickness direction) is imposed for all nodes along both ends as shown in Fig. 2. At the fixed end, all nodes are also constrained in the 1-direction (the axial direction). At the loaded end, a fixed load is applied, while requiring the end to remain straight and parallel to its unloaded direction; this condition is imposed using constraint equations. These boundary conditions are considered to be the most accurate representation of the constraints imposed by the grips of the testing machine. This highly constrained and symmetric condition for the double-lap joint means that the effects of geometric non-linearity are small. This

contrasts with the single lap joint when these effects are highly significant, e.g. [4]. Despite the small effect, non-linear geometry was used for all the analyses.

The mesh was drawn using 8-noded quadratic elements. The maximum ratio of element width:length was 1:2 within the adhesive and 1:8 within the adherends. A typical mesh contained around 5400 elements.

4.2. Material modelling

The material properties of the unidirectional laminate were obtained from the manufacturer's data sheet. Transverse isotropy was assumed. The properties used are shown in Table 1, where the subscript L designates the longitudinal (fibre) direction and the subscript T designates the transverse direction.

The value of longitudinal modulus was checked using a dynamic method, with a beam vibrating in flexural free-free mode; the measured value of 131 GPa is in good agreement with the value from the data sheet.

The elastic material properties of the adhesive used were those measured in previous work [2]: $E = 2.497\,\text{GPa}$, $v = 0.4$. For most of the analyses reported here elastic–plastic material properties were used for the adhesive. From this previous work, the measured tensile stress/strain curve of the adhesive and measured values of Poisson's ratio with tensile strain were available.

These measured properties clearly show that the plastic behaviour of the adhesive cannot be modelled using the simple von Mises criterion. The value of Poisson's ratio decreases with increasing strain; the von Mises criterion assumes that plastic strain takes place at constant volume, with a Poisson's ratio of 0.5. Further, the behaviour of the adhesive is expected to be pressure sensitive. The plastic behaviour of the adhesive was therefore modelled using the Drucker-Prager model available in ABAQUS. A simple model was defined with a linear tip to the yield cone, and associated flow.

The model was derived using the measured values of Poisson's ratio [5]. The best fit between the measured overall value of Poisson's ratio and the value predicted for different values of plastic Poisson's ratio was sought. The best fit around yield was found using a value of Plastic Poisson's ratio of 0.32. This value, ν_{pl} was used to calculate the angle, φ, in the Drucker-Prager model using:

$$\tan\ \varphi = \frac{3(1 - 2\nu_{pl})}{2(1 - \nu_{pl})}. \tag{1}$$

Assuming associated flow ($\varphi = \beta$) the values required for the Drucker-Prager model can then be defined as

$$A = 22.5^\circ$$
$$K = 1$$
$$\varnothing = 22.5^\circ$$

The behaviour of this material model was tested using a simple finite element model. The model was subjected to unidirectional stress; the results are shown in Fig. 3a and compared with the experimental results. Good agreement was found. The simple Drucker-Prager model is therefore confirmed to be a reasonably accurate model of the behaviour.

The sensitivity of the material model to hydrostatic stress was demonstrated by subjecting the finite element model to pure hydrostatic stress. The results are shown in Fig. 3b. Yielding in pure hydrostatic stress occurs at around 150 MPa. This value is rather high, but it is important to note that yielding under pure hydrostatic stress never occurs for material modelled using the von Mises yield criterion. The maximum hydrostatic stress found in the simulations is around 80 MPa, which would be expected to cause failure.

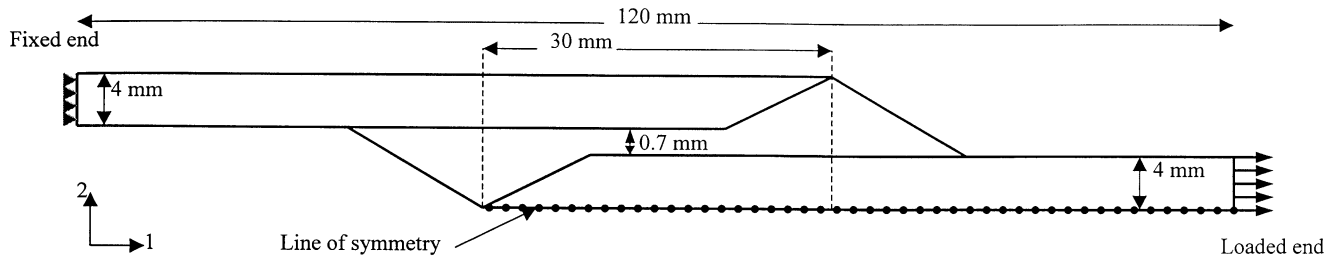

Fig. 2. Geometry of the finite element model.

Table 1
Material properties of unidirectional laminate

E_L (GPa)	E_T (GPa)	ν_{LT}	ν_{TT}	G_{LT} (GPa)	G_{TT} (GPa) ..
133	9.3	0.3	0.3	4.88	3.56

5. Modelling of crack growth in the finite element simulations

Cracks were introduced into the mesh by renumbering nodes of adjacent elements. Crack tip elements were not used as point values of stress at the crack tip are not meaningful. The real crack length is probably always longer than that simulated.

The preferred direction of crack growth in the Mode I direction can be deduced from examination of the vectors of maximum principal stress. The virtual crack growth method [6] can be applied. This method for assessing energy release rate is based on the concept that the energy released in growing the crack is equal to the energy which would be required to close the crack. Forces and displacements at the crack tip are found from finite element simulations and calculations of energy can subsequently be made. The shape of the growing crack can be used as a further indication of the likely direction of further crack growth.

5.1. Crack growth in unmodified adhesive

Two different paths of crack growth for the unmodified adhesive have been modelled in the finite element simulations, representing the extreme cases observed experimentally. The two paths are illustrated in Fig. 4. For both paths, the crack initiates at the tip of the upper adherend and runs perpendicular to the fillet. This path is expected to be perpendicular to the maximum principal stress, and therefore will be the preferred direction of crack growth. For the 'straight' crack path, the crack runs along this straight line towards the bottom of the bondline. For the 'curved' crack path, the crack curves along the centre of the bondline. Results have been obtained for the crack positions shown by A B C for the straight crack, and A B K I for the curved crack path (Fig. 4). The two initial positions, A and B, are identical for both paths, representing 1.3 and 2.5 mm of crack growth, respectively. For the straight path the crack growth continues in a straight line to position C which is 0.35 mm from the interface. For the curved crack growth the path curves through position B and then proceeds in a horizontal direction to position I, both positions at the centre of the bondline; position I is directly below the corner of the fillet.

5.2. Crack growth in modified adhesive

Both the Kapton™ film layer and nylon cloth were introduced along the centre of the bondline, as indicated in Fig. 5; this idealised position was used in the simulations. The presence of the layer or cloth were not explicitly included in the finite element models. This is justified since the material properties of the Kapton™ layer are not well known, but are expected to be very close to the properties of the adhesive. The nylon cloth used was a very light mesh which would be very readily penetrated by the adhesive. Further, the properties of the adhesive and the polyamide are likely to be similar. The crack positions investigated in the simulations are shown on Fig. 5. As described in Part I [1], crack growth in the joints modified with the Kapton™ layer initiated at the upper adherend corner, similarly to the crack growth in unmodified joints. However, crack growth in the joints modified using the nylon mesh initiated within

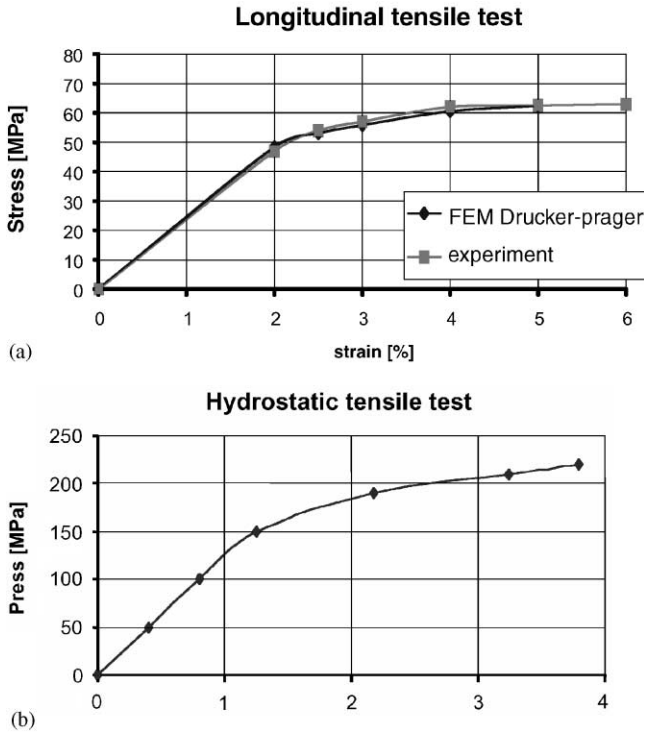

Fig. 3. Derivation of the Drucker-Prager material model: (a) comparison of experimental and predicted tensile stress/strain curves and (b) predicted response to hydrostatic tensile stress.

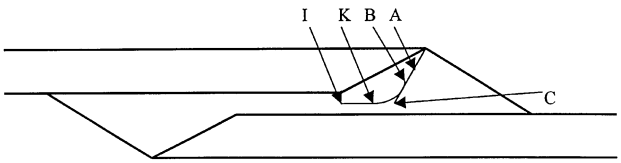

Fig. 4. Simulated crack paths for the unmodified adhesive.

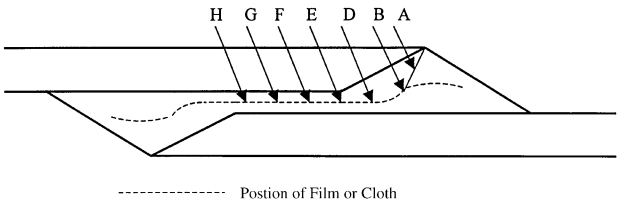

Fig. 5. Simulated crack paths for the modified adhesives.

the bondline around point E (Fig. 5), which is directly under the corner of the adherend. Subsequent crack growth was observed to occur towards the fillet, along the path E–B. This crack path has been examined in the finite element simulations.

6. Finite element results

All results from the simulations are presented for a 48 kN applied load, which is a typical quasi-static failure load for these joints.

6.1. Results for unmodified adhesive

Observations of the vectors of maximum principal stress as the crack grew towards position B confirmed that this crack growth direction is perpendicular to the maximum principal stress. For the straight crack path towards the interface to position C (Fig. 4), the path continues perpendicular to the maximum principal stress. When the crack is in this position, through-thickness stresses of about 50 MPa in the inner adherend are found. The contour plot of through-thickness stress is shown in Fig. 6. The overall continuity of through-thickness stress across the interfaces indicates the accuracy of this simulation.

As noted above, the precise values of stress around the crack tip are not reliable. However, below the crack tip, within the adherend, is a separate region of stress concentration which is sufficiently remote from the crack tip that the values are reliable. It is notable that these values of through-thickness stress could be sufficiently high to cause transverse failure in composite laminates.

The curved crack path deviates from the path perpendicular to the maximum principal stress. The contours of through-thickness stress are similar to those for the straight crack. For both crack paths, the value of through-thickness stress increases with crack growth. These values occur in the region of adherend under the fillet, as shown in Fig. 6. The value of the peak stress, which exceeds 50 MPa, has been shown experimentally to cause transverse failure of similar materials [7].

The observed straight direction of crack growth from position B has been confirmed by calculations of fracture energy using the virtual crack growth method [6]. The energy was calculated at point B for continuing straight crack growth or subsequent curved crack growth. The results are shown in Table 2.

It should be noted that the values calculated are the 'Total' values, without separation of Mode I and II.

Table 2
Energy release rate for different crack paths for unmodified adhesive

crack path	G (J/m^2)
straight	1630
curved	1390

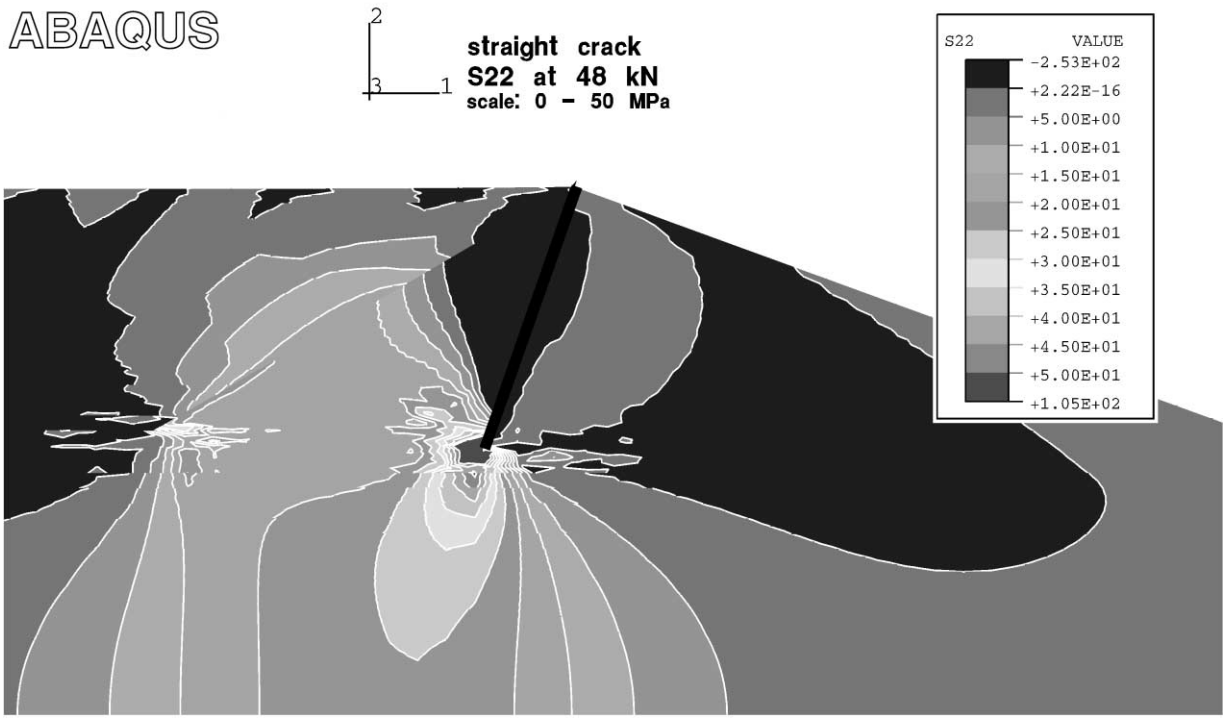

Fig. 6. Contour plot of through-thickness stress for a straight crack at position C.

This calculation indicates that more energy is released when the crack continues straight to the inner adherend. Diverting the crack into a curve would mean less released energy and is therefore a less probable crack path. The mode I energy release rate for EC 3448 has been measured using a tapered double cantilever beam; the measured value was $1100\,J/m^2$ [8]. This measured value is within the same range as the predicted values shown in Table 2 noting that the measurements and predictions have been obtained using very different geometries.

The experimental results show a crack path which is between the two models analysed here. The finite element simulations indicate that the straighter crack path is most likely. The simulations confirm the experimental observations that crack growth along the bondline is not expected for the joints with unmodified adhesive. When the crack reaches the lower adherend, the experimental observations showed that delamination of the inner adherend occurs. The predicted values of transverse stress are sufficiently high that transverse failure would be expected. The processes of crack growth and failure of the joint have been well simulated by the finite element models.

6.2. Crack growth in adhesive modified by Kapton^{tm} film

The presence of the film was simulated by the diversion of the crack along the path of the modelled location (Fig. 5). The position E is in the centre of the bondline, directly below the corner of the fillet. Although the crack growth was simulated along the bond line, to position H, the numerical results are not reliable since the symmetry assumption is not applicable, particularly for these long crack lengths. However, we note that the symmetry condition assumed here is the 'worst case' condition with cracking occurring on both sides of the joint.

The crack has been diverted by the presence of the film at position D (Fig. 5). Observation of the vectors of maximum principal stress show that the crack is growing in a mixed mode including Mode II. The contours of through-thickness stress when the crack has reached position D are shown in Fig. 7. Comparing Figs. 6 and 7, it can be seen that the maximum value of transverse stress in the adherend is reduced by the diversion of the crack. The transverse stress in the adherend for the diverted crack is unlikely to be sufficiently high to cause delamination. These observations from the simulations confirm the experimental observation that delamination of the inner adherend does not cause joint failure for the joints made using adhesive modified with Kapton^{TM} film.

Values of energy release rate for the different crack positions were calculated using the Virtual Crack Growth method. The results are shown in Table 3. The value at position D is lower than the value at position C (Fig. 4) indicating that the crack diversion is caused by the presence of the film. Further crack growth beyond position D indicates very high values of energy release rate owing to the high shear stress. A crack which has grown beyond position D is expected to propagate.

The results of the finite element simulations including the crack diversion caused by the Kapton^{TM} film are in agreement with the experimental observations. The diversion of the crack arises from the modification by the film, and causes the crack to grow in mixed mode, including Mode II. This crack diversion suppresses the delamination of the inner adherend. As shown by the experimental results, the crack grows within the bondline to a measurable length before failure of the joint.

6.3. Crack growth in adhesive modified by nylon mesh

The nylon mesh was inserted in the bond line in a similar position to that of the Kapton^{TM} film, as shown in Fig. 5. As used for the modification by Kapton^{TM} film, the presence of the mesh was modelled by simulation of the experimentally observed crack growth.

The experimentally observed failure mode for the adhesive modified by the nylon mesh is different from that described above, where the crack started at the outer edge of the fillet. For the joints made using adhesive modified by nylon mesh, the initial crack growth is an internal crack, formed by separation around the mesh close to position E (Fig. 5). Subsequent crack growth occurs along the bondline and finally towards the outer edge of the fillet around point A (Fig. 5).

These processes were examined using finite element simulations. The site of the initial crack growth was examined for the presence of stress concentrations which could cause the initial internal crack growth. The position of internal crack growth was found to coincide with the maximum shear stress in the bondline. This is seen from the contours of shear stress in the adhesive shown in Fig. 8. The presence of the nylon mesh could cause a reduction in shear strength of the adhesive, leading to the formation of an internal crack at this position.

Table 3
Values of energy release rate calculated for different crack positions in Kapton^{TM} film modified adhesive

Position	G (J/m^2)
A	577
B	1230
C	1690
D	1340

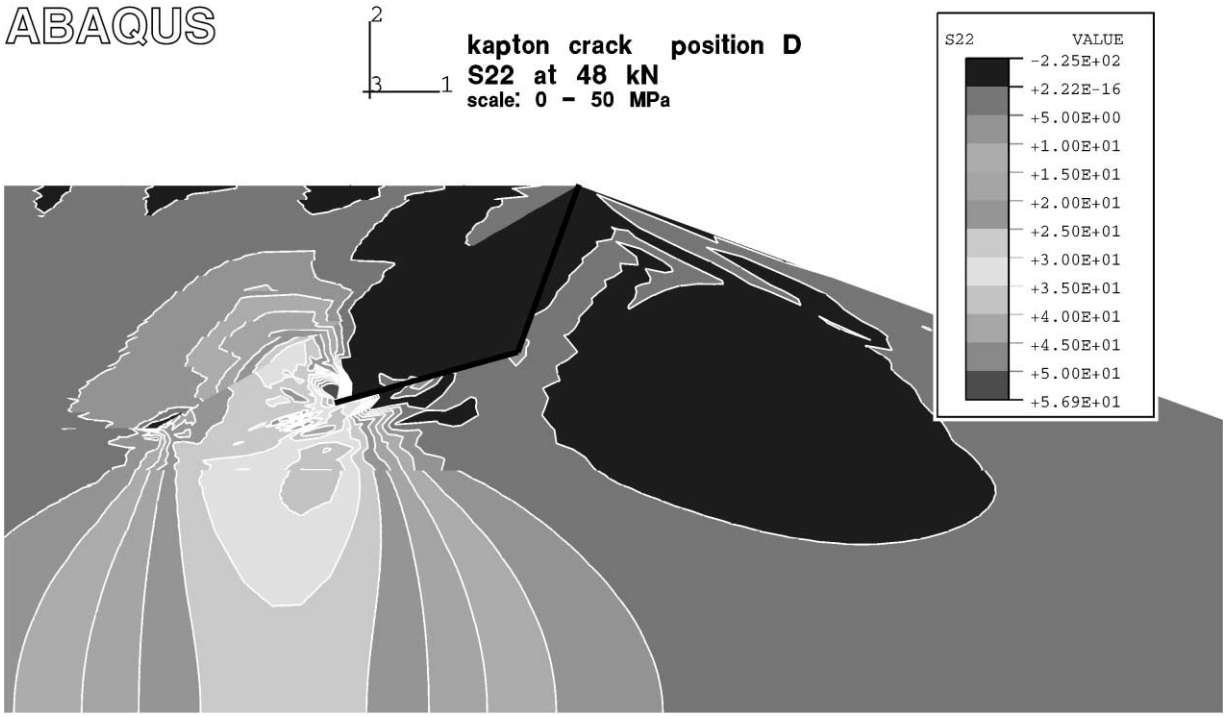

Fig. 7. Contour plot of through-thickness stress for a crack diverted by Kapton^{TM} film, at position D.

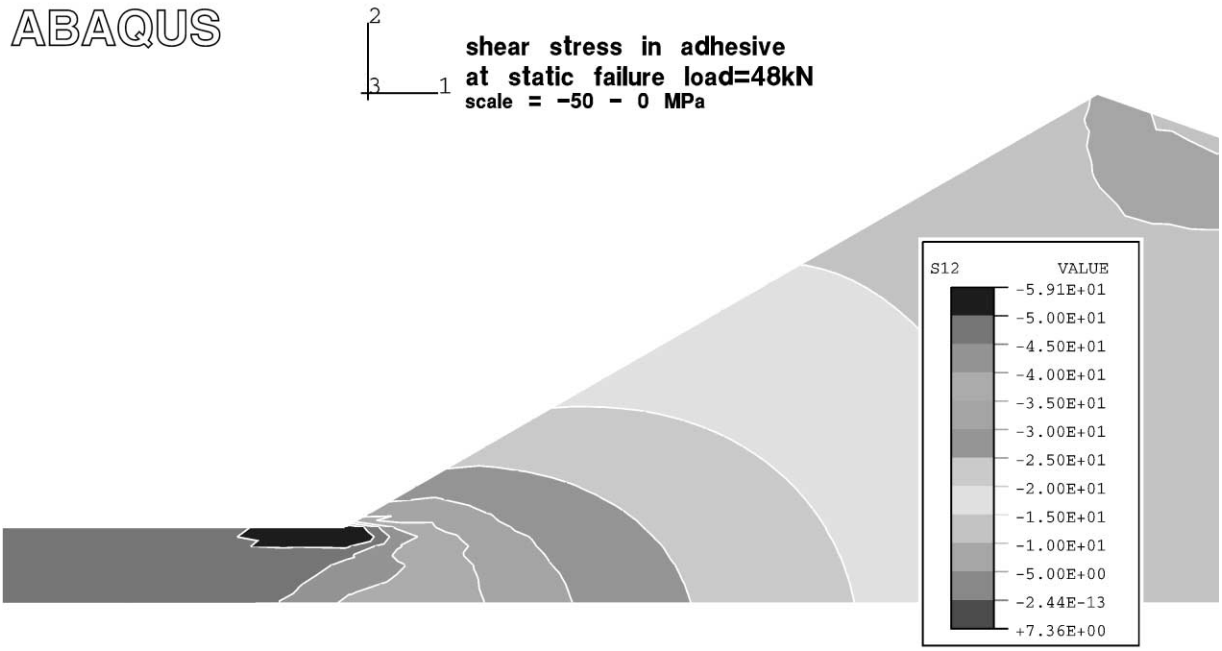

Fig. 8. Contour plot of maximum shear stress in the adhesive showing stress concentration around the initiation of the internal crack.

The presence of the internal crack was then simulated. The vectors of maximum principal stress around the internal crack show that direction of preferred crack growth, in Mode I direction, is indicated to be towards the fillet. This result is further shown by examination of the shape of the crack, shown in Fig. 9. The maximum

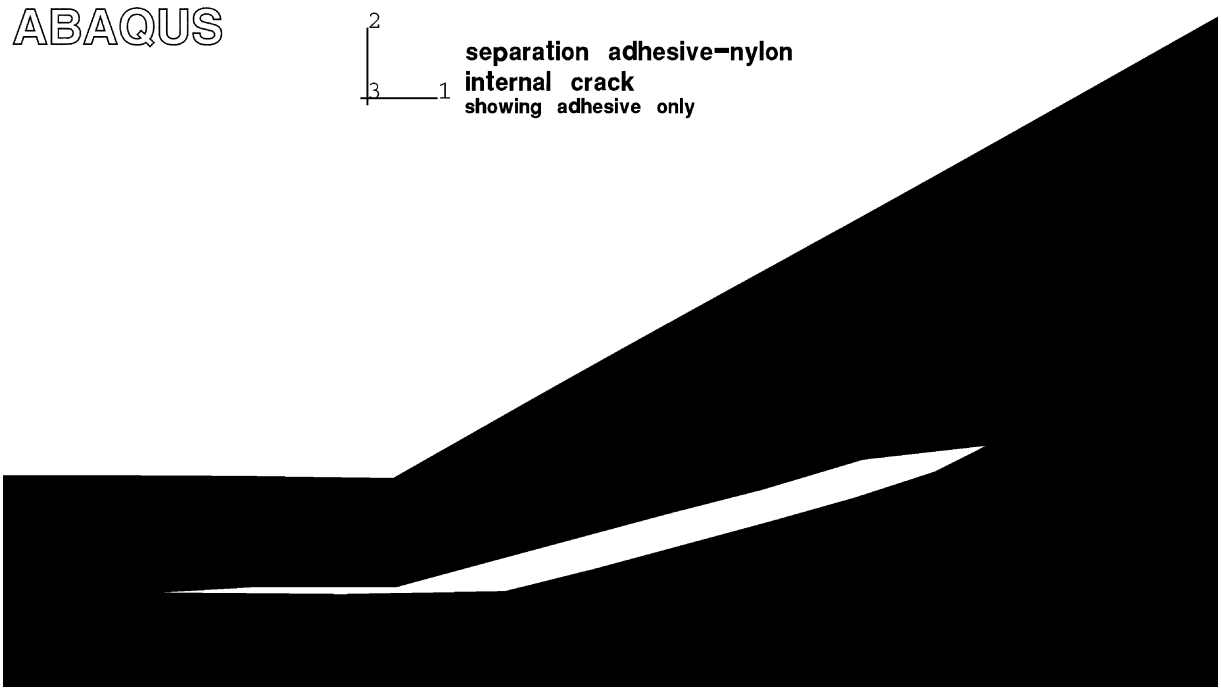

Fig. 9. Simulated crack shape for the internal crack.

crack opening displacement is towards the fillet end of the crack, indicating that crack growth would be expected in this direction.

The finite element simulations of the failure processes in the adhesive modified by the nylon mesh have accurately described the observed failure process and their sequence. The internal crack initiation is predicted to arise from the concentration of shear stress in that position in the bondline. Further crack growth towards the fillet, as observed experimentally, is predicted in the simulations. Results from the simulations indicate that crack growth towards the lower adherend would not occur. Thus high transverse stress in the through-thickness direction in the lower adherend, which could cause delamination, is not expected to occur in these joints.

7. Conclusions

The results from the finite element simulations have accurately described the failure process observed experimentally. For joints made using the unmodified adhesive, the experimentally observed crack growth through the fillet to the inner adherend has been confirmed as the expected crack path. This crack growth has been shown to cause high values of transverse, through-thickness, stress in the inner adherend, with sufficiently high values which would be expected to lead to delamination. The experimentally observed failure process for these joints was catastrophic delamination of the inner adherend. Results from the simulations indicated that crack growth along the bondline would not be expected without significant modification of the adhesive layer forcing the crack along that path.

Significant modification of the adhesive layer was provided by including a layer of Kapton^{TM} film or nylon mesh within the bondline. These modifications diverted the crack along the centre of the bondline, preventing the high transverse stress arising in the inner adherend. The experimentally observed crack growth processes for the different modifications were different, reflecting the different failure strengths. The crack initiated at the outer corner of the fillet for the joint made using adhesive modified by Kapton^{TM} film, but internal crack growth was observed for the joint made with adhesive modified by nylon mesh. Both types of crack growth have been accurately simulated.

The accuracy of these simulations confirms the experimental results. Modification of the adhesive in joints made with composite adherends can force the crack to grow along the bondline. Catastrophic failure via delamination of the adherends is prevented. These results are very important for confident use of adhesive joints between composite adherends in engineering applications.

Acknowledgements

This work was funded by BAE SYSTEMS Airbus UK Ltd and the input of Airbus UK staff into the programme discussions is gratefully acknowledged.

References

[1] Potter KD, Guild FJ, Harvey HJ, Wisnom MR, Adams RD. Understanding and control of adhesive crack propagation in bonded joints between carbon fibre composite adherends, Part I experimental. Int J Adhes Adhes 2001;21:435.
[2] Towse A, Potter KD, Wisnom MR, Adams RD. Specimen size effects in the tensile failure strain of an epoxy adhesive. J Mater Sci 1998;33:4307.
[3] Thomas R, Garcia I, Guild FJ, Adams RD. Adhesive joining of composite laminates. Plast Rubber Compos Process Appl 1998;27:200.
[4] Adams RD, Comyn J, Wake WC. Structural adhesive joints in engineering. London: Chapman & Hall, 1997.
[5] Duncan BC, Dean GD, Read BE. Prediction of the performance of adhesives under impact Loading. Proc. SAE V, Bristol, UK, 1998 (IOM).
[6] Rybicki EF, Kanninen MF. A finite element calculation of stress intensity factors by a modified crack closure integral. Eng Fract Mech 1977;9:931.
[7] Hiel CC, Sumich M, Chappell DP. Determining a laminate's interlaminar tensile strength using a curved beam test specimen. J Compos Mater 1991;25:854.
[8] Kinloch AJ. Private communication (1998).